Langmuir

Article

pubs.acs.org/Langmuir

Transformation of Indium Nanoparticles to β-Indium Sulfide: Digestive Ripening and Visible Light-Induced Photocatalytic Properties

Sreeram Cingarapu,[†] Myles A. Ikenberry,[‡] Dambar B. Hamal,[†] Christopher M. Sorensen,[§] Keith Hohn,[‡] and Kenneth J. Klabunde*,[†]

[†]Department of Chemistry, [‡]Department of Chemical Engineering, and [§]Department of Physics and Kansas State University, Manhattan, Kansas 66506, United States

Supporting Information

ABSTRACT: We report the transformation of polydispersed dodecanethiol stabilized indium nanoparticles, obtained from bulk indium shot by evaporation/condensation solvated metal atom dispersion (SMAD) technique, into highly monodispersed partially alkyl thiolate-capped β-indiumsulfide (In_2S_3) by a postpreparative digestive ripening in high boiling point *t*-butyltoluene (190 °C) solvent. Upon digestive ripening, the as-prepared polydispersed black indium nanoparticles showed a characteristic color transition from black to cream, pale yellow, yellow, and finally to brown, indicating the transformation of the indium metal nanoparticles into intermediates composed of indium thiolates, sulfides, and polysulfides, and finally into the product In_2S_3 nanoparticles whose surfaces are partially capped with thiolates. The transformed product (In_2S_3) was characterized with UV−vis, XRD, EDX, SEM, XPS, and TEM. From XRD and TEM measurements, the average size of the transformed In_2S_3 nanoparticles is 5 nm. The optical absorbance of the as-prepared sample showed absorption peaks around 538 and 613 nm; upon digestive ripening these two peaks disappeared and stabilized at 375 nm, providing evidence of strong quantum confinement of excitons. The visible light-induced photocatalytic activity test with the In_2S_3 nanoparticles showed that 95% of Rhodamine B (RhB) dye degraded after 100 min of irradiation with visible light.

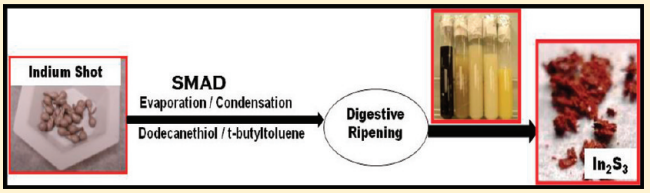

INTRODUCTION

Indium sulfide is a III−VI group semiconductor. It has two composite forms, InS and In_2S_3, with band gaps of 2.44[1] and 2.0−2.2 eV,[2] respectively, and this corresponds to an absorption wavelength of 550−620 nm.[3] At atmospheric pressure, In_2S_3 is found to crystallize into three different structural forms, defective cubic structure (α-In_2S_3), defective spinel structure (β-In_2S_3), and layered hexagonal structure (γ-In_2S_3). Among these three forms, β-In_2S_3 has gained much attention because of its unique electronic,[4] optical,[5] optoelectronic,[6] and semiconductor sensitization[7] properties. Furthermore, β-In_2S_3 has been used as a buffer layer in solar cells,[8] a heterojunction in photovoltaic electric generators,[9] a photocatalytic material for hydrogen evolution[10−13] and biological imaging sensors,[14] and a photocatalytic material for the degradation of dyes.[15,16]

There are several ways of synthesizing β-In_2S_3; one direct way is by high temperature treatment of sulfur and indium elements in a quartz vessel.[17] Other methods include heating In_2O_3 in the presence of H_2S gas,[18] sonochemical treatment,[19] solvent reduction,[20] thermal decomposition of a single-source precursor,[21] hydrothermal,[22] and laser induced synthesis.[23] Usually the sulfur is provided either by sulfides (for example Li_2S,[24] Na_2S_3,[25] NaHS,[26] H_2S[27]), sulfur powder,[9] sodium thiosulfate,[20] dimethyl sulfoxide,[27] thioacetamide,[19] thioglycolic acid,[28] sulfonate,[29] CS_2,[30] thiourea,[31] L-cystine,[32] sulfur-oleylamine complex,[33] or thiols.[34]

In recent years, metal alkanethiolates have been used as precursor molecules for the synthesis of metal and metal sulfides by thermal decomposition at moderately low temperatures (120−200 °C) either in solvents or in solvent free conditions. For example, Carotenuto et al. reported "a general method to synthesize metal or metal sulfide clusters embedded in polymer matrices".[35] Korgel et al. reported the solventless synthesis of nickel sulfide and copper sulfide by decomposing corresponding thiolate precursors in the presence of octanoate,[36,37] and Nakamoto et al. reported the synthesis of gold nanoparticles by thermal decomposition of gold thiolate precursors.[38,39] Most recently Zhong et al. reported "the synthesis of copper sulfide from ultra fine thiol-capped copper nanoclusters by a thermally activated route".[40]

Recently our group has reported the synthesis of indium nanoparticles by the metal evaporation/co-condensation SMAD technique, followed by digestive ripening under mild conditions (38 °C) in the presence of excess amine and phosphine ligands.[41] In this current work we describe the use of

Received: September 15, 2011
Revised: January 14, 2012
Published: January 24, 2012

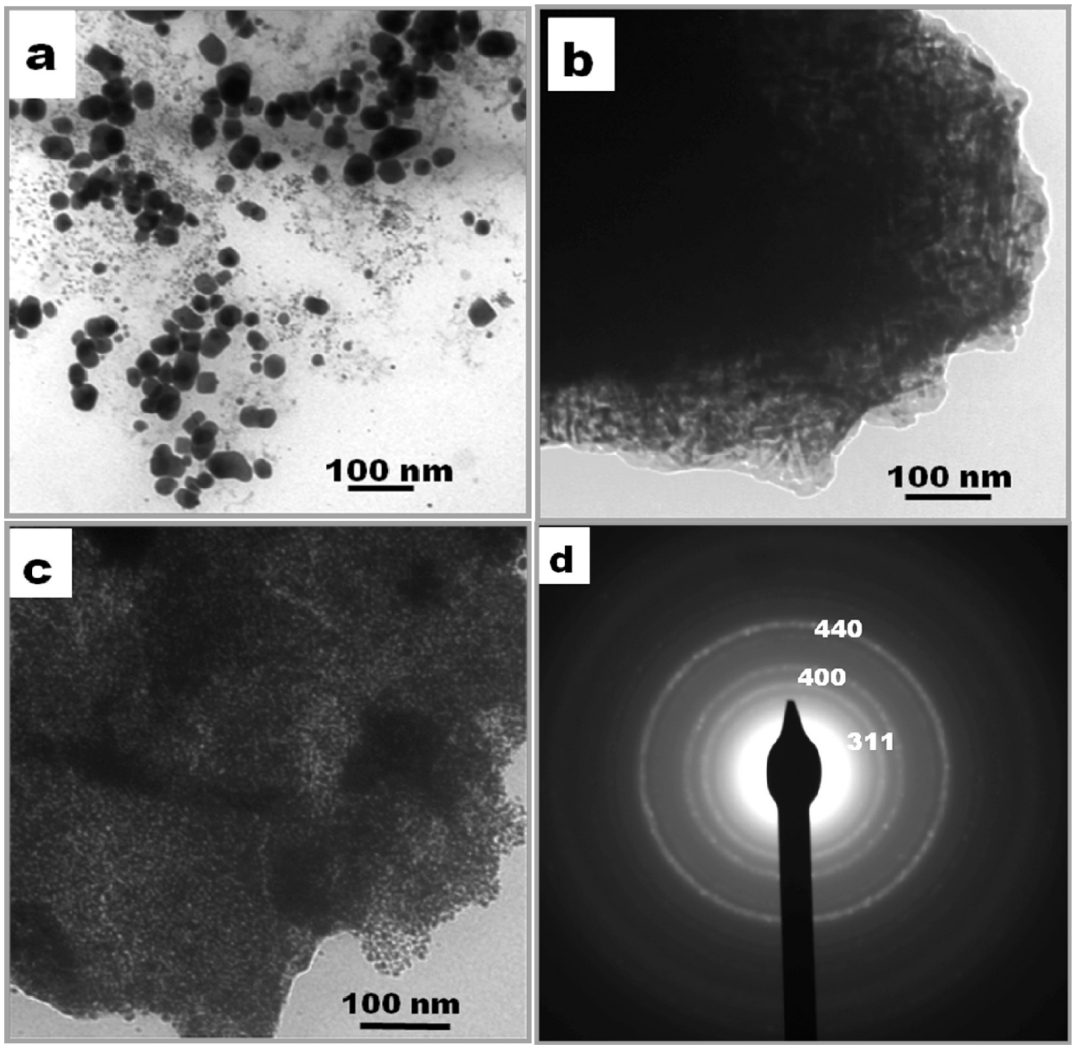

Figure 1. (a) As-prepared SMAD indium-dodecanethiol, (b) intermediate product obtained after 30 min of digestive ripening, (c) indium sulfide nanoparticles obtained after 4 h of digestively ripening, and (d) corresponding ED from the indium sulfide nanoparticles.

dodecanethiol ligand and digestive ripening at an elevated temperature (190 °C) under the protection of argon. This process is more than merely digestive ripening; it is a novel way of synthesizing β-indium sulfide nanoparticles. The photocatalytic properties of these β-indium sulfide (In_2S_3) nanoparticles were investigated with Rhodamine B (RhB) dye degradation under visible light irradiation.

EXPERIMENTAL SECTION

Materials required indium shot (99.9%, Strem Chemicals Inc.), dodecanethiol ≥98%, rhodamine B (95%), *t*-butyltoluene (TBT) 99% (Alfa Aesar), methylene chloride (Fisher Scientific), acetone (Fisher Scientific), and ethanol (Absolute, 200 Proof, Aaper Alcohol and Chemical Co.) were used as received without further purification with the exceptions that TBT was purged with argon for 2 h prior to use, and methylene chloride was distilled and degassed four times by the standard freeze−thaw procedure prior to the reaction.

Synthesis of As-Prepared Indium Nanoparticles by Evaporation and Co-Condensation SMAD Technique. In a typical synthesis, a stationary reactor was used as described previously.[42] 0.3 g of indium shot was charged into a C9 boron nitride crucible (R.D. Mathis # C9-BN) resting in a metal basket (R. D. Mathis # B8B # x.030 w) and the entire setup was then covered with insulating packing material (Zircar product, Inc.) to dissipate the heat generated during the metal evaporation. This crucible was then connected to water cooled copper electrodes. Dodecanethiol was then charged into the SMAD reactor (in a 1:30 metal to ligand ratio) along with 60 mL of *t*-butyl toluene. After vacuum sealing the entire setup, a liquid N_2 Dewar was placed around the sealed SMAD reactor. Once the vacuum attained a pressure of 4×10^{-3} Torr, 50 mL of distilled and degassed methylene chloride (Fisher chemicals) was evaporated through a solvent shower head, which was inserted into the reactor. Evaporated solvent condensed on the wall of the SMAD reactor (which was cooled by the external liquid nitrogen), and gradual resistive heating elevated the temperature of the reactor until it approached the temperature required for the metal vaporization (900 °C). After nearly 2 h, the metal had been vaporized completely, and simultaneous co-condensation of the metal and solvent (100 mL of methylene chloride) restricted the condensed metal particles from aggregation. The matrix was then allowed to melt at room temperature under vigorous stirring and mixing with dodecanethiol ligand, resulting in an indium colloid which was black in appearance. After siphoning the product into a Schlenk tube under argon, the solvent methylene chloride was vacuum evaporated to leave behind the indiumdodecanethiol-TBT colloid.

Digestive Ripening. The as-prepared indium-dodecanethiol-TBT colloid was then subjected to digestive ripening at the boiling point of the TBT solvent (190 °C) for 4 h in an argon atmosphere. Digestive ripening is a postpreparative treatment used to make monodispersed particles from polydispersed colloidal particles in the presence of excess ligands upon heating the colloid near or at the boiling point of

dx.doi.org/10.1021/la203624p | *Langmuir* 2012, 28, 3569−3575

the solvent.[43−48] In the current work, we adopted the same technique and transformed SMAD-prepared polydispersed indium metal nanoparticles into monodispersed indium sulfide semiconductor nanoparticles whose surfaces are partially capped with thiolates. The samples were washed with copious amount of absolute ethanol and acetone and then vacuum-dried before TEM, SEM and XPS analysis.

Visible Light Photocatalytic Activity Test. In order to investigate the visible light photocatalytic activity of β-In_2S_3, RhB dye was chosen as probe molecules. Photocatalytic experiments were performed in a 300 mL cylindrical glass reactor (Supporting Information (SI) Figure S1) with a quartz window and the temperature was maintained at 25 °C by water circulation. The light source was an Oriel 1000-W high-pressure Xe lamp. The combined optical glass filters were used to eliminate ultraviolet radiation for visible light catalysis (>420 nm). At first, 39 mg of β-In_2S_3 was placed at the bottom of the glass reactor. Then, 100 mL of 2×10^{-5} M aqueous solution of rhodamine B (RhB) dye was added to the catalytic reactor. Before shining visible light, the catalyst and RhB dye solution were stirred for 120 min to establish adsorption−desorption equilibrium. Then 3 mL of dye solution was extracted from the reactor for the UV−vis measurement by a Carry 500 UV−vis spectrometer to follow the degradation reaction of the dye under dark and light conditions. After each UV−vis analysis, the sample was returned to the reactor.

Characterization. *UV−Vis Spectroscopy.* UV−vis absorption spectra were obtained using a Cary 500 Scan UV−vis−NIR spectrophotometer. Nanoparticle samples were washed with copious amounts of absolute ethanol, acetone, and were dried under vacuum. The dried samples were then redissolved in toluene for analysis.

Transmission Electron Microscopy (TEM). TEM studies were performed on a Philips CM100 operating at 100 kV. The TEM samples were prepared by placing a few micro liters of sample (which was precipitated, washed with copious amount of ethanol an acetone, vacuum-dried and redissolved in toluene) onto carbon-coated Formvar copper grids, and the grids were allowed to dry overnight. The facilities were provided by the Microscopy and Analytical Imaging Laboratory at Department of Biology, Kansas State University.

Powder X-ray diffraction (XRD). Powder X-ray diffraction patterns were recorded by a Bruker D8 X-ray diffractometer with CuKα radiation. XRD samples were prepared by the evaporation of toluene from the sample/toluene dispersion loaded on XRD glass plates. The samples were scanned from $10 < 2\theta < 70°$ at an increment of 0.01°/min and the total acquisition time period was more than 6 h.

Scanning Electron Microscope (SEM) with Energy-Dispersive X-ray (EDX) Analyzing System. SEM analysis was performed using an S3500N, Hitachi Science System, Ltd. at the Entomology Department of Kansas State University, which was also used to measure the EDX spectrum so as to determine the surface composition of the samples under conditions of 20 keV. Prior to SEM and EDX analysis, all samples were precipitated, washed with copious amounts of ethanol and acetone and, then redispersed in ethanol.

X-ray Photoelectron Spectroscopy (XPS). XPS data were recorded using a Perkin−Elmer PHI 5400 electron spectrometer using polychromatic Al Kα radiation (1486.6 eV). Analysis was carried under vacuum less than 2×10^{-8} Torr. The XPS binding energies were measured with a precision of 0.1 eV. The analyzer pass energy was set to 17.9 eV, and the contact time was 50 ms. The spectrometer was calibrated by setting the binding energies of Au $4f_{7/2}$ and Cu $2p_{3/2}$ to 84.0 and 932.7 eV, respectively. The sample spectra were referenced to the adventitious C_{1s} peak at 285.0 eV. For XPS analysis, all samples were precipitated with ethanol, washed with copious amount of acetone and then vacuum-dried.

RESULTS AND DISCUSSION

The as-prepared SMAD product was black in color and with digestive ripening turned lighter dark, then yellow, then dark yellow, and finally (after a total of 4 h of digestive ripening) into a dark brown precipitate (SI, Figure S2 (a-f)). At room temperature, these samples appear like gel; upon addition of ethanol, the precipitated sample has a fiber-like appearance (SI, Figure S2(g)), and this fibrous material is easily redissolved in toluene. As-prepared SMAD product has a broad UV−vis absorption peak ranging from 550 to 610 nm (SI, Figure S3) but within 15 min of digestive ripening the UV−vis peak shifts to 375 nm and stabilizes at the same wavelength. This spectral shift indicates a strong quantum confinement of the excitonic transmission expected for the In_2S_3 nanoparticles.[49] The position (375 nm) of the absorption band correlates well with the UV−vis characteristic peak of In_2S_3 nanoparticles prepared by other groups.[14]

The as-prepared SMAD indium nanoparticles had a large size distribution (Figure 1a) due to the agglomeration of indium metal during the vaporization and co-condensation process. However, after 30 min of digestive ripening the obtained intermediate appears like an aggregate of polydisperse particles as seen in Figure 1b (note: the polymer-like fiber shown in SI, Figure S2(g) resulted after precipitation with ethanol). Based on the XPS analysis, the intermediates are most likely a mixture of indium thiolates, sulfides, and polysulfidic species. During prolonged (4 h) digestive ripening, the indium metal nanoparticles are transformed eventually into In_2S_3 nanoparticles partially capped with thiolates (the brown final product SI, Figure S2(f)), whose TEM image is shown in Figure 1c. Histograms of as-prepared SMAD indium nanoparticles and In_2S_3 nanoparticles obtained after digestive ripening are provided in the Supporting Information (SI, Figure S3 (a) and (b)). From the electron diffraction (Figure1d), the final product displays polycrystalline rings that can be indexed to the (311), (400), and (440) facets, which are in agreement with the intense diffraction peaks from the X-ray powder diffraction (XRD).

Figure 2 shows the XRD diffraction peaks revealing the crystal structure of the final product. All reflection peaks were

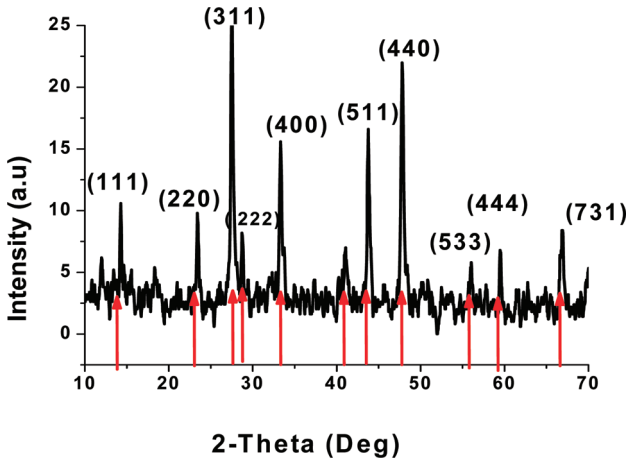

Figure 2. XRD patterns of the final product. All of the diffraction peaks can be indexed to the β-In2S3 with a = 10.77 Å (JCPDS 65-0459).

carefully compared with the Joint Committee on Powder Diffraction Standards (JCPDS 65−0459) data file and identified as the β- phase of In_2S_3 with a = 10.77 Å. The observed peak position at 2θ = 14.32°, 23.38°, 27.41°, 28.52°, 33.38°, 43.73°, 47.75°, 55.81°, 59. 29°, and 67° were indexed as (111), (220), (311), (222), (400), (511), (440), (533), (444),

dx.doi.org/10.1021/la203624p | Langmuir 2012, 28, 3569−3575

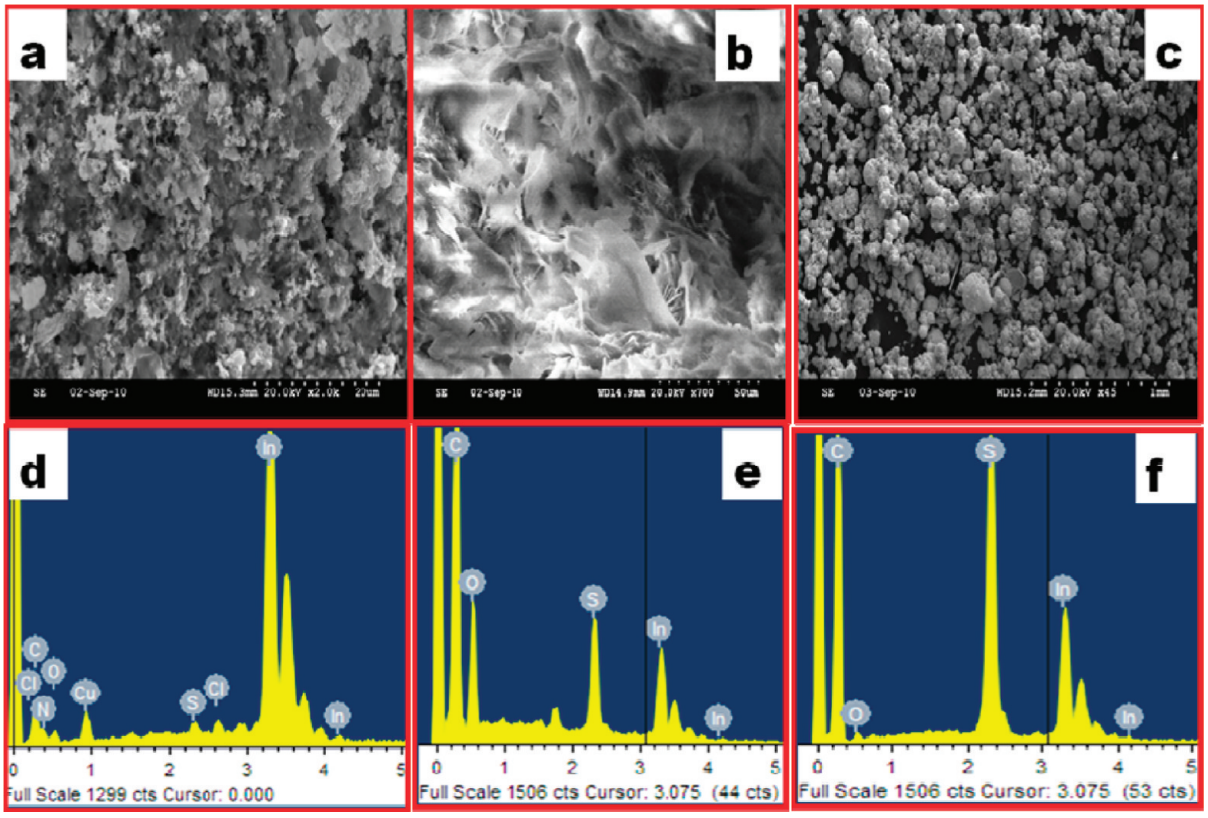

Figure 3. Scanning electron microscope (SEM) image and energy dispersion X-ray (EDX) microanalysis and elemental mapping of (a and d) as-prepared indium-dodecanethiol showing mainly indium metal, (b and e) intermediate compound obtained after 1 h of digestive ripening (note the appearance of carbon and sulfur peaks) and, (c and f) the final product showing both sulfur and indium.

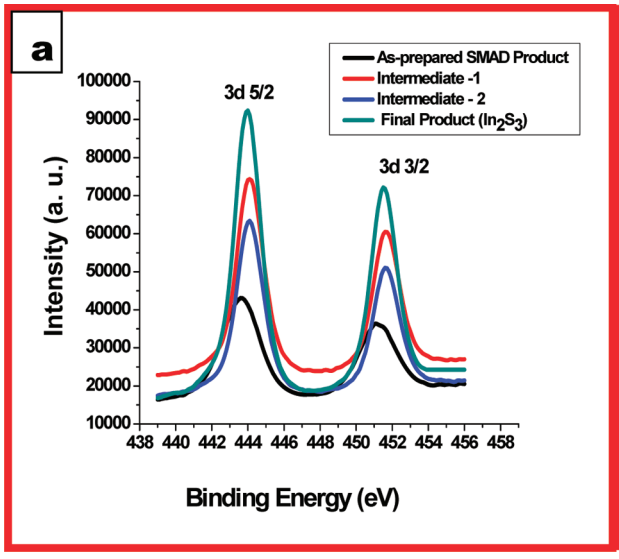

b

	$In3d_{3/2}$ peak (eV)	FWHM
SMAD	452.0	2.1
Int. 1	452.6	1.6
Int. 2	452.6	1.6
Final product		
	452.5	1.5
Reference In_2S_3		
	452.5	1.2

Figure 4. Binding energy spectrum of the as-prepared indium-dodecanethiol (before digestive ripening), intermediate compounds (obtained after digestive ripening 30 and 60 minutes), and final product (In_2S_3). (a) $In3d_{5/2}$ and $In3d_{3/2}$ XPS spectra. (b) $In3d_{3/2}$ peak positions and FWHM.

and (731), respectively. The sharp XRD pattern is due to larger particles not easy to distinguish in the TEM images.

Panels a–c in Figure 3 are the SEM images of the as-prepared SMAD indium-dodecanethiol after 1 h of digestive ripening and the final product respectively. The energy dispersive X-ray (EDX) microanalysis and elemental mapping have been carried out by SEM. The EDX spectrum in Figure 3d shows that the as-prepared SMAD product predominantly consists of indium. Although the metal to ligand ratio was 1:30, the absence of sulfur in the SMAD product is most likely due to the loss of both unbound and weakly bound thiol ligands during the rigorous washing procedure that was adopted due to the gel nature of the materials. However, after 30 min of digestive ripening, the appearance of sulfur along with carbon (Figure 3e) indicates the formation of an intermediate containing alkyl thiolates. The final product (Figure 3f)

dx.doi.org/10.1021/la203624p | *Langmuir* 2012, 28, 3569–3575

composed of sulfur and indium, and the ratio of sulfur to indium atoms was 1:1.58 and this value is close to the theoretical values of 1.5 expected for In_2S_3. Further, the obtained ratio of sulfur to indium atoms (1:1.58) matched well with the group 12 sulfides formed by thermal decomposition of metal-complexes in high-boiling point solvents.[50−52] The trace amount of oxygen in Figure 3d,e might be from the solvent used for the SEM sample preparation. Figure 3e shows an increased oxygen presence that may correspond to increased solvent retention in the amorphous regions of the intermediate material.

X-ray Photoelectron Spectrometry (XPS) measurements were carried out to further investigate the composition and chemical state of the as-prepared SMAD product, the intermediate species, and the final product. All peak fittings were carried with the XPSPEAK41 software employing a Tougaard background correction and 80:20 Lorentzian:Gaussian peaks. For investigation of each sample's $S2p_{3/2}$ region and $In3d_{3/2}$ region, separate peak fittings were carried out with the number of assigned major peaks varying from one to three.

Indium XPS Analysis. The $In3d_{3/2}$ peak of the SMAD product had a peak at 452.0 eV (Figure 4a,b), indicating that indium was present in the form of indium metal. The binding energy of bulk indium metal $3d_{3/2}$ orbital is around 451.2 eV,[50] although Balamurgan et.al have found that the binding energy increases along with a decrease in the size of indium metal nanoparticles.[53] For intermediate 1 (30 min of digestive ripening), intermediate 2 (60 min of digestive ripening), and the final product, analysis of the $In3d_{3/2}$ peaks shown in Figure 4a,b indicates that the binding energy of surface indium atoms immediately increases upon digestive ripening, corresponding with rapid oxidation of the indium metal into In^{3+}.

Sulfur XPS Analysis. As other authors have noted, the fwhm of the sulfur 2p peaks complicates resolution and quantification of the thiolate species.[54] A further complication involves the tendency of thiol peaks to shift and for sulfur content to decrease under X-ray irradiation.[55,56] The software XPSPEAK41 was used to fit one, two, or three $S2p_{3/2}$ peaks to each sample, with each $S2p_{3/2}$ peak assigned a corresponding $S2p_{1/2}$ peak with a binding energy 1.2 eV higher and an area fixed at 50% of the $S2p_{3/2}$ area. Additionally, in an attempt to account for the lack of certainty regarding the fwhm, each $S2p_{3/2}$ peak fitting had two separate optimizations: the first employed a fixed fwhm of 1.0 eV for all peaks, and the second allowed the fwhm of each peak to be optimized by the software. The peak fitting gave consistent binding energy determinations regardless of whether the fwhm is fixed or allowed to vary, although the areas assigned to each peak varied significantly. This result may indicate that the XPS analysis yields useful information regarding the states of sulfur in each sample, but also that there remains a significant uncertainty in the quantification of how much sulfur exists in each state. Optimized peak fittings with fixed fwhm of each sample's $S2p_{3/2}$ region are given in the Supporting Information (SI, Figures S5−S9).

Comparing with other literature,[14,23,55,57−61] and with a reference indium sulfide sample, XPS analysis indicates that there are three states of sulfur corresponding to polysulfide, thiolate, and indium sulfide with $S2p_{3/2}$ binding energies of approximately 163.2, 162.3, and 161.6 eV, respectively (Table 1). Based on the solubility, the polysulfide present in the intermediates might be a cyclic (tiara) alkanethiolate compound because metal alkanethiolates have been found to be insoluble in organic solvents, and to have layered structures (for example Ag,[55,62,63] Pb,[64,65] and Cu[66]). Additionally those which are soluble in organic solvents have cyclic structures.[67−70] Efforts to grow crystals from these intermediates have not been successful in our hands.

Table 1. $S2p_{3/2}$ Peak Fitting Binding Energies of the As-Prepared Indium-Dodecanethiol (Before Digestive Ripening), Intermediate Compounds (Obtained after Digestive Ripening 30 and 60 Minutes), Final Product, and Reference In_2S_3 Sample[a]

	$S2p_{3/2}$ peak fittings	
	B.E. (eV)	fwhm
SMAD	161.6	1
	163.3	1
int. 1	161.7	1
	162.4	1
	163.1	1
int. 2	161.7	1
	162.3	1
	163	1
final	161.6	1
product	162.4	1
reference In_2S_3	161.6	1

[a]See the Supporting Information for peak fitting images.

Peak assignments for sulfur species can be seen in Table 1. The SMAD product had only a trace amount of sulfur, and the corresponding $S2p_{3/2}$ peak fitting was therefore tentative. The best fit was attained with two $S2p_{3/2}$ peaks at binding energies of 161.6 and 163.3 eV. These two peaks indicate the presence of sulfidic and polysulfidic species on the surface of the SMAD indium nanoparticles. It is uncertain whether the sulfides formed during X-ray irradiation of polysulfide or thiolate species on the SMAD particles surfaces.

Intermediate 1 was best fit with three $S2p_{3/2}$ peaks with binding energies of 161.7, 162.4, and 163.1 eV (Table 1). These energies are associated with indium sulfide, thiolate, and polysulfide species, respectively. Intermediate 2 was also best fit with three $S2p_{3/2}$ peaks, at 161.7, 162.3, and 163.0 eV (Table 1).

The final product was best fit with two $S2p_{3/2}$ peaks at 161.6 and 162.4 eV, indicating the presence of sulfide and thiolate species, and the absence of polysulfides. The presence of alkyl thiolate species in the final product is further confirmed by a significant carbon concentration as seen in the XPS survey composition analysis (not shown).

The XPS and XRD data indicate that the digestive ripening process allows the dodecanethiol ligand to quickly react with the indium metal nanoparticles and oxidize the indium metal into In^{3+}. Further changes during the digestive ripening process involve the rearrangement and reduction of the sulfur species along with breakage of C−S bonds. No change in C−S infrared spectrum was found when thiol was heated in the absence of nanoparticles, which also supported that the C−S breakage occurred in the presence of In_2S_3 (see the SI, Figure S10 for the IR spectrum of DDT before and after heating). The intermediates contain polysulfide, thiolate, and sulfide species, while the final product is composed of monodisperse indium sulfide nanoparticles with indium thiolate present on the surface. An overall picture that emerges is of indium reacting with the dodecanethiol ligand and transforming, via thermally activated digestive ripening and indium-catalyzed interfacial C−

dx.doi.org/10.1021/la203624p | Langmuir 2012, 28, 3569−3575

S cleavage reactions, into crystalline β-In_2S_3 nanoparticles whose surfaces are partially capped with indium thiolate. The process and final product are similar to the recently published synthesis of copper sulfide nanodiscs.[40] A possible reaction sequence for the transformation of indium metal to In_2S_3 is as follows.

$$In(0) + 3HSCH_2CH_2R \rightarrow In(SCH_2CH_2R)_3 + 3/2H_2 \quad (1)$$

$$2In(SCH_2CH_2R)_3 \rightarrow In_2S_3 + H_2S + 2CH_2{=}CHR + 2RCH_2CH_2SCH_2CH_2R \quad (2)$$

Visible Light Photodegradation of Organic Dyes. To further investigate the visible light photocatalytic activity of β-In_2S_3, 29 mg of In_2S_3 was used for the photodegradation of RhB. Many research groups have used RhB as a model pollutant because it exhibits absorbance maxima at 552 nm and the decrease in the absorbance at 552 nm reflects the dye degradation (Figure 5). However, Zhao et al have reported that

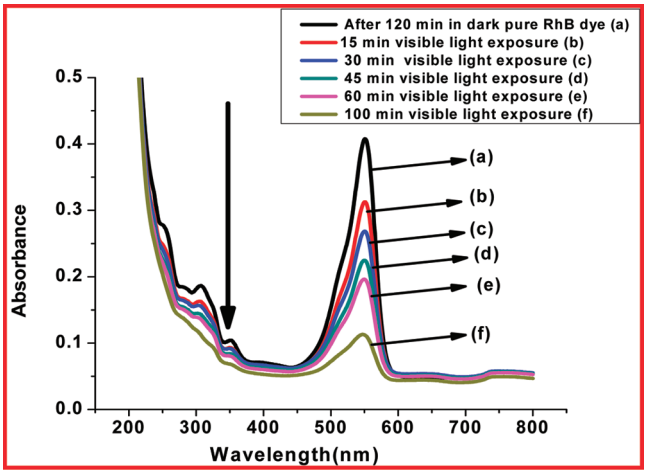

Figure 5. Shows the spectral change of RhB/In_2S_3 dispersion under visible light irradiation, the initial concentration of RhB is 2×10^{-5} M. The arrow refers to the de-alkylation. (a) Pure RHB dye and (b–f) degradation of RhB with the exposure time.

RhB de-ethylation (300 nm) is mainly a surface reaction, whereas RhB chromophore ring degradation (552 nm) is mainly due to a solution bulk process.[71,72] Hence, the fast de-ethylation of RhB indicates the photocatalyzed degradation of the dye molecule as shown in Figure 5. After being illuminated under visible light for 60 min, the RhB decreases by 96%. Rhodamine B (RhB) is a non-azo cation dye that is commonly used to test photoactivity because it has a tendency to undergo photocatalytic reaction due to the photoinduced conduction band electrons and become colorless under visible light illumination.

We also carried out 2 control experiments under the same experimental condition: (1) with RhB dye alone and (2) RhB with dodecanethiol (5 drops in 100 mL of dye solution; SI, Figure S11). The outcomes of these experiments are as follows. (a) RhB dye does not undergo the self-photodegradation reaction even though the dye has the ability to absorb the visible light photons. This proves that the degradation of RhB dye was not mediated by its self-sensitizing properties. (b) RhB dye did not degrade in the presence of the thiol ligand under visible light, indicating that the thiol does not play a catalytic role in the photodegradation of RhB dye. Thus, RhB photodegradation reactions confirm the photocatalytic activity of In_2S_3.

CONCLUSIONS

Polydispersed, dodecanethiol-stabilized indium nanoparticles obtained from bulk indium metal by evaporation/condensation SMAD technique were transformed by a postpreparative digestive ripening process in high boiling point solvent into highly monodispersed β-In_2S_3 nanoparticles with surfaces partially capped by thiolates. The UV–vis measurements confirmed the strong quantum confinement effect of β-In_2S_3 nanoparticles, and the XRD, XPS, and EDX further confirmed the formation of alkyl thiolate capped β-In_2S_3 nanoparticles.

The partial capping of nanoparticle surfaces by alkanethiolates does not prevent the photocatalytic activity. The visible light-induced photocatalytic activity test indicated that the transformed product is a potential photocatalyst for the degradation of pollutant molecules similar to Rhodamine B. The post preparative digestive ripening was shown to be highly effective for the conversion of polydispersed indium metal nanoparticles into photocatalytic, alkanethiolate capped β-In_2S_3 nanocrystals.

ASSOCIATED CONTENT

Supporting Information

Visible light photocatalytic dye degradation experimental set up, series of samples showing the transformation, UV–vis spectrum, IR spectrum of dodecanethiol before and after heating, XPS curve fitting of the SMAD product's S2p3/2 orbital data, intermediate 1 with three S2p3/2 peaks fitting, intermediate 2 with three S2p3/2 peaks fittings, final product with two S2p3/2 peaks fitting, and XPS of reference In2S3 are provided. This material is available free of charge via the Internet at http://pubs.acs.org.

AUTHOR INFORMATION

Corresponding Author

*Phone: 785-532-6849. Fax: 785-532-6666. E-mail: kenjk@ksu.edu.

Notes

The authors declare no competing financial interest.

ACKNOWLEDGMENTS

The support of NSF (CT 50609318) and DOE (DE-SC0005159) is gratefully acknowledged. Also, we thank Dr. Dan Boyle for assistance with transmission electron microscopy and also Prashant Chopade for helping with IR spectrum.

REFERENCES

(1) Nishino, T.; Hamakawa, Y. *Jpn. J. Appl. Phys.* **1977**, *16*, 1291–1300.

(2) Timoumi, A.; Bouzouita, H.; Kanzari, M.; Rezig, B. *Thin Solid Films* **2005**, *480- 481*, 124–128.

(3) Nagesha, D. K.; Liang, X.; Mamedov, A. A.; Gainer, G.; Eastman, M. A.; Giersig, M.; Song, J.-J.; Ni, T.; Kotov, N. A. *J. Phys. Chem. B* **2001**, *105*, 7490–7498.

(4) Kamoun, N.; Belgacem, S.; Amlouk, M.; Bennaceur, R.; Bonnet, J.; Touhari, F.; Nouaoura, M.; Lassabatere, L. *J. Appl. Phys.* **2001**, *89*, 2766–2771.

(5) Choe, S.-H.; Bang, T.-H.; Kim, N.-O.; Kim, H.-G.; Lee, C.-I.; Jin, M.-S.; Oh, S.- K.; Kim, W.-T. *Semicond. Sci. Technol.* **2001**, *16*, 98−102.
(6) Kim, W. T.; Kim, C. D. *J. Appl. Phys.* **1986**, *60*, 2631−2633.
(7) Yasaki, Y.; Sonoyama, N.; Sakata, T. *J. Electroanal. Chem.* **1999**, *469*, 116−122.
(8) Dalas, E.; Sakkopoulos, S.; Vitoratos, E.; Maroulis, G.; Kobotiatis, L. *J. Mater. Sci.* **1993**, *28*, 5456−60.
(9) Dalas, E.; Kobotiatis, L. *J. Mater. Sci.* **1993**, *28*, 6595−6597.
(10) Kudo, A.; Nagane, A.; Tsuji, I.; Kato, H. *Chem. Lett.* **2002**, 882−883.
(11) Naik, S. D.; Jagadale, T. C.; Apte, S. K.; Sonawane, S.; Kulkarni, M. V.; Patil, S. I.; Ogale, S. B.; Kale, B. B. *Chem. Phys. Lett.* **2008**, *452*, 301−305.
(12) Osterloh, F. E. *Chem. Mater.* **2008**, *20*, 35−54.
(13) Fu, X. L.; Wang, X. X.; Chen, Z. X.; Zhang, Z. Z.; Li, Z. H.; Leung, D. Y. C.; Wu, L.; Fu, X. Z. *Appl. Catal., B* **2010**, *2010, 95*, 393−399.
(14) Nagesha, D. K.; Liang, X.; Mamedov, A. A.; Gainer, G.; Eastman, M. A.; Giersig, M.; Song, J.-J.; Ni, T.; Kotov, N. A. *J. Phys. Chem. B* **2001**, *105*, 7490−7498.
(15) Du, W. M.; Zhu, J.; Li, S. X.; Qian, X. F. *Cryst. Growth Des.* **2008**, *8*, 2130−2136.
(16) He, Y. H.; Li, D. Z.; Xiao, G. C.; Chen, W.; Chen, Y. B.; Sun, M.; Huang, H. J.; Fu, X. Z. *J. Phys. Chem. C* **2009**, *113*, 5254−5262.
(17) Kaito, C.; Saito, Y.; Fujita, K. *J. Cryst. Growth* **1989**, *94*, 967−77.
(18) Bube, R. H.; McCarroll, W. H. *J. Phys. Chem. Solids* **1959**, *10*, 333−335.
(19) Avivi, S.; Palchik, O.; Palchik, V.; Slifkin, M. A.; Weiss, A. M.; Gedanken, A. *Chem. Mater.* **2001**, *13*, 2195−2200.
(20) Xiong, Y.; Xie, Y.; Du, G.; Tian, X. *J. Mater. Chem.* **2002**, *12*, 98−102.
(21) Afzaal, M.; Malik, M. A.; O'Brien, P. *Chem. Commun.* **2004**, 334−335.
(22) Vigneashwari, B.; Dash, S.; Tyagi, A. K.; Parameswaran, P.; Ravichandran, V.; Sunthathiraraj, S. A. *J. Nanosci. Nanotechnol.* **2007**, *7*, 2087−2091.
(23) Asikainen, T.; Ritala, M.; Leskelae, M. *Appl. Surf. Sci.* **1994**, *82/83*, 122−5.
(24) Nosaka, Y.; Ohta, N.; Miyama, H. *J. Phys. Chem.* **1990**, *94*, 3752−5.
(25) Kumta, P. N.; Phule, P. P.; Risbud, S. H. *Mater. Lett.* **1987**, *5*, 401−4.
(26) Kamat, P. V.; Dimitrijevic, N. M.; Fessenden, R. W. *J. Phys. Chem.* **1988**, *92*, 2324−9.
(27) Gao, P.; Xie, Y.; Chen, S.; Zhou, M. *Nanotechnology* **2006**, *17*, 320−324.
(28) Chen, W.; Bovin, J.-O.; Joly, A. G.; Wang, S.; Su, F.; Li, G. *J. Phys. Chem. B* **2004**, *108*, 11927−11934.
(29) Dutta, D. P.; Sharma, G.; Ghoshal, S.; Kushwah, N. P.; Jain, V. K. *J. Nanosci. Nanotechnol.* **2006**, *6*, 235−240.
(30) Xiong, Y.; Xie, Y.; Du, G.; Tian, X.; Qian, Y. *J. Solid State Chem.* **2002**, *166*, 336−340.
(31) Zhu, X.; Ma, J.; Wang, Y.; Tao, J.; Zhou, J.; Zhao, Z.; Xie, L.; Tian, H. *Mater. Res. Bull.* **2006**, *41*, 1584−1588.
(32) Chen, L.-Y.; Zhang, Z.-D.; Wang, W.-Z. *J. Phys. Chem. C* **2008**, *112*, 4117−4123.
(33) Kim, Y. H.; Lee, J. H.; Shin, D. W.; Park, S. M.; Moon, J. S.; Nam, J. G.; Yoo, B. *Chem. Commun.* **2010**, *46*, 2292−2294.
(34) Dutta, D. P.; Sharma, G.; Tyagi, A. K.; Kulshreshtha, S. K. *Mater. Sci. Eng., B: Solid-State Mater. Adv. Technol.* **2007**, *138*, 60−64.
(35) Carotenuto, G.; Martorana, B.; Perlo, P.; Nicolais, L. *J. Mater. Chem.* **2003**, *13*, 2927.
(36) Ghezelbash, A.; Sigman, M. B.; Korgel, B. A. *Nano Lett.* **2004**, *4*, 537−542.
(37) Larsen, T. H.; Sigman, M. B.; Ghezelbash, A.; Doty, R. C.; Korgel, B. A. *J. Am. Chem. Soc.* **2003**, *125*, 5638.
(38) Nakamoto, M.; Yamamoto, M.; Fukusumi, M. *Chem. Commun.* **2002**, 1622−1623.
(39) Nakamoto, M.; Kashiwagi, Y.; Yamamoto, M. *Inorg. Chim. Acta* **2005**, *358*, 4229−4236.
(40) Mott, D.; Yin, J.; Engelhard, M.; Loukrakpam, R.; Chang, P.; Miller, G.; Bae, I.- T.; Chandra Das, N.; Wang, C.; Luo, J.; Zhong, C.-J. *Chem. Mater.* **2009**, *22*, 261−271.
(41) Cingarapu, S.; Yang, Z. Q.; Sorensen, C. M.; Klabunde, K. J. *Inorg. Chem.* **2011**, *50*, 5000−5005.
(42) Klabunde, K. J. T., P. L.; Skell, P. S.; Ittel, S. *Inorg. Synth.* **1979**, *19*, 59−86.
(43) Lin, X. M.; Sorensen, C. M.; Klabunde, K. J. *J. Nanopart. Res.* **2000**, *2*, 157−164.
(44) Stoeva, S.; Klabunde, K. J.; Sorensen, C. M.; Dragieva, I. *J. Am. Chem. Soc.* **2002**, *124*, 2305−2311.
(45) Smetana, A. B.; Klabunde, K. J.; Sorensen, C. M. *J. Colloid Interface Sci.* **2005**, *284*, 521−526.
(46) Heroux, D.; Ponce, A.; Cingarapu, S.; Klabunde, K. J. *Adv. Funct. Mater.* **2007**, *17*, 3562−3568.
(47) Prasad, B. L. V.; Stoeva, S. I.; Sorensen, C. M.; Klabunde, K. J. *Langmuir* **2002**, *18*, 7515−7520.
(48) Prasad, B. L. V.; Stoeva, S. I.; Sorensen, C. M.; Klabunde, K. J. *Chem. Mater.* **2003**, *15*, 935−942.
(49) Lavrent'ev, A.; Safontseva, N.; Dubeiko, V.; Gabrel'yan, B.; Nikiforov, I. *Phys. Solid State* **2000**, *42*, 2047−2053.
(50) Laine, E.; Tamminen, M.; Mäkelä, R.; Pessa, M. *J. Mater. Sci.* **1983**, *18*, 295−298.
(51) Malik, M. A.; Revaprasadu, N.; O'Brien, P. *Chem. Mater.* **2001**, *13*, 913−920.
(52) Trindade, T.; O'Brien, P.; Zhang, X.-m. *Chem. Mater.* **1997**, *9*, 523−530.
(53) Balamurugan, B.; Kruis, F. E.; Shivaprasad, S. M.; Dmitrieva, O.; Zahres, H. *Appl. Phys. Lett.* **2005**, *86*, 3.
(54) Pleth Nielsen, L.; SchÃnning, M.; Christensen, S. V.; Hoffmann, S. r. V.; Li, Z.; Hofmann, P.; Besenbacher, F.; Clausen, B. S. *Catal. Lett.* **2001**, *73*, 85−90.
(55) Bensebaa, F.; Zhou, Y.; Deslandes, Y.; Kruus, E.; Ellis, T. H. *Surf. Sci.* **1998**, *405*, L472−L476.
(56) Zerulla, D.; Chasse, T. *Langmuir* **1999**, *15*, 5285−5294.
(57) Wu, Z.; Ma, D. K.; Zhen, H.; Tang, Q.; Xie, O.; Qian, Y. T. *J. Nanosci. Nanotechnol.* **2005**, *5*, 776−780.
(58) Nielsen, L. P.; Schonning, M.; Christensen, S. V.; Hoffmann, S. V.; Li, Z. S.; Hofmann, P.; Besenbacher, F.; Clausen, B. S. *Catal. Lett.* **2001**, *73*, 85−90.
(59) Castner, D. G.; Hinds, K.; Grainger, D. W. *Langmuir* **1996**, *12*, 5083−5086.
(60) Bourg, M.-C.; Badia, A.; Lennox, R. B. *J. Phys. Chem. B* **2000**, *104*, 6562−6567.
(61) Smart, R. S. C.; Skinner, W. M.; Gerson, A. R. *Surf. Interface Anal.* **1999**, *28*, 101−105.
(62) Baena, M. J.; Espinet, P.; Lequerica, M. C.; Levelut, A. M. *J. Am. Chem. Soc.* **1992**, *114*, 4182.
(63) Dance, I. G.; Fisher, K. J.; Herath Banda, R. M.; Scudder, M. L. *Inorg. Chem.* **1991**, *30*, 183.
(64) Shaw, R. A.; Woods, M. *J. Chem. Soc. A* **1971**, *10*, 1569.
(65) Tiers, G. V. D.; Brostrom, M. L. *J. Appl. Crystallogr.* **2000**, *33*, 915.
(66) Sandhyarani, N.; Predeep, T. *J. Mater. Chem.* **2001**, *11*, 1294.
(67) Gould, R. O.; Harding, M. M. *J. Chem. Soc. A* **1970**, 875.
(68) Ivanov, S. A.; Kozee, M. A.; Merrill, W. A.; Agarwal, S.; Dahl, L. F. *J. Chem. Soc., Dalton Trans.* **2002**, 4105.
(69) Kunchur, N. R. *Acta Crystallogr.* **1968**, *B24*, 1623.
(70) Woodward, P.; Dahl, L. F.; Abel, E. W.; Crosse, B. C. *J. Am. Chem. Soc.* **1965**, *87*, 5251.
(71) Wu, T.; Liu, G.; Zhao, J.; Hidaka, H.; Serpone, N. *J. Phys. Chem. B* **1998**, *102*, 5845−5851.
(72) Zhao, J.; Wu, T.; Wu, K.; Oikawa, K.; Hidaka, H.; Serpone, N. *Environ. Sci. Technol.* **1998**, *32*, 2394−2400.